



This is a repository copy of *Structure of some CoCrFeNi and CoCrFeNiPd multicomponent HEA alloys by diffraction techniques.*

White Rose Research Online URL for this paper:  
<http://eprints.whiterose.ac.uk/108947/>

Version: Accepted Version

---

**Article:**

Dahlborg, U., Cornide, J., Calvo-Dahlborg, M. et al. (5 more authors) (2016) Structure of some CoCrFeNi and CoCrFeNiPd multicomponent HEA alloys by diffraction techniques. *Journal of Alloys and Compounds*, 681. pp. 330-341. ISSN 0925-8388

<https://doi.org/10.1016/j.jallcom.2016.04.248>

---

Article available under the terms of the CC-BY-NC-ND licence  
(<https://creativecommons.org/licenses/by-nc-nd/4.0/>)

**Reuse**

This article is distributed under the terms of the Creative Commons Attribution-NonCommercial-NoDerivs (CC BY-NC-ND) licence. This licence only allows you to download this work and share it with others as long as you credit the authors, but you can't change the article in any way or use it commercially. More information and the full terms of the licence here: <https://creativecommons.org/licenses/>

**Takedown**

If you consider content in White Rose Research Online to be in breach of UK law, please notify us by emailing [eprints@whiterose.ac.uk](mailto:eprints@whiterose.ac.uk) including the URL of the record and the reason for the withdrawal request.



[eprints@whiterose.ac.uk](mailto:eprints@whiterose.ac.uk)  
<https://eprints.whiterose.ac.uk/>

# **Structure of some CoCrFeNi and CoCrFeNiPd multicomponent HEA alloys by diffraction techniques**

U. Dahlborg<sup>1</sup>, J. Cornide<sup>1</sup>, M. Calvo-Dahlborg<sup>1,\*</sup>, T.C. Hansen<sup>2</sup>, A. Fitch<sup>3</sup>, Z. Leong<sup>4</sup>, S. Chambreland<sup>1</sup>, R. Goodall<sup>4</sup>

<sup>1</sup>*GPM-UMR6634-CNRS, University of Rouen, Campus Madrillet, BP12, 76801 Saint-Etienne-du-Rouvray, France*

<sup>2</sup>*Institut Laue-Langevin, 71 Avenue des Martyrs, CS 20156, 38042 Grenoble Cedex 9, France*

<sup>3</sup>*ESRF, 71 Avenue des Martyrs, CS40220, 38043 Grenoble Cedex 9, France*

<sup>4</sup>*Department of Materials Science & Engineering, The University of Sheffield, Mappin Street, Sheffield S1 3JD, UK*

**\*Corresponding author:** M. Calvo-Dahlborg email: [monique.calvo-dahlborg@univ-rouen.fr](mailto:monique.calvo-dahlborg@univ-rouen.fr)

## **Abstract**

The structure of  $\text{CoCrFe}_y\text{Ni}$  ( $y=0, 0.8$  and  $1.2$ ) and  $\text{CoCrFeNi-Pd}_x$  ( $x= 0.0, 0.5, 0.8, 1.0, 1.2$  and  $1.5$ ) High Entropy Alloys has been investigated by neutron and standard X-ray as well as by high-energy X-ray diffraction techniques. The alloys were produced by arc melting and afterwards heat treated under several different conditions. It has been concluded that the  $\text{CoCrFeNi}$  alloy in as-cast condition is, contrary to what is claimed in the literature, not single-phase but consists of at least two different phases, both of fcc type. The difference in lattice constant between the two phases is close to  $0.001 \text{ \AA}$ . Diffraction patterns measured by X-ray and neutron diffraction have shown that the structure of the alloy is not affected by 3 hours heat treatment up to  $1100^\circ\text{C}$ . Changing the amount of Fe has no drastic effect on alloy structure. The Pd-containing alloys have also all been found not to be single-phase but to consist of at least four different phases, all being of fcc type. The lattice constants for all phases increase with Pd content. The relative amounts of the different phases depend on Pd concentration. Furthermore, heat treatments of three hours duration at different temperatures have a significant effect on the alloy phase composition. It is suggested that HEAs should be considered as multicomponent alloys presenting “simple” diffraction patterns, e.g. consisting of one or several lattices of fcc, hcp or bcc type with very close lattice parameters.

**Key words:** HEA, diffraction,  $\text{CoCrFeNiPd}$ , multicomponent, structure, fcc

## 1. Introduction

Multicomponent metallic alloys of the type usually called High Entropy Alloys (HEAs) have recently raised considerable attention because of their attractive physical properties [1-6] such as high hardness, outstanding wear resistance, good high-temperature strength and thermal stability. A HEA was originally defined as an alloy consisting of 5 or more components of relative compositions in the range 5 to 35 at.% forming single and simple close-packed crystalline structures of solid solution type [7]. However, there are very few, if any, HEAs that are truly single phase. Many of the alloys taken to meet the current definition of a HEA alloy are in reality multiphase with in most cases one main phase and one or several minor phases [8,9]. Thus, the original definition of a HEA has to be reconsidered and several approaches to this have been made (see for example [10,11]). From the literature and the authors' own experience HEAs should be considered as multicomponent alloys presenting "simple" diffraction patterns, e.g. consisting of one or several lattices of fcc or bcc type with very close lattice parameters. The alloys that are discussed below correspond to this definition and will irrespective of their actual compositions, be denoted as HEAs.

Numerous publications have been devoted to finding rules by which it is possible to predict whether an alloy of a certain composition forms a HEA upon solidification. Suggested models based on semi-empirical approaches have considered both electronic quantities such as the elemental electronegativities, concentrations of valence electrons and the itinerant electron concentrations d-orbital energy levels and also thermodynamic ones such as the enthalpy and the entropy of mixing of the binaries that can be formed by the elements [12-21]. The parameters have been combined with the atomic size mismatch of the elements in order to predict if an alloy is of HEA type via statistical methods [22-25 and references therein]. Furthermore, CALPHAD [5, 10, 26-28], DFT and *ab initio* [29-31] calculations have been used for the same purpose. The main difficulty met for the validation of models and calculations is that measured structures and microstructures and also physical properties published in the literature show a considerable spread. This circumstance suggests that the alloys in many cases have not been adequately characterized in terms of possible small contents of intermetallic phases and grain size distributions depending on different production techniques and thermal treatments. In order to

resolve this situation it is obviously necessary to use different complementary experimental techniques covering a length scale from a tenth of a nanometer to several microns.

One well reported family of HEAs is based on the four component CoCrFeNi (below denoted CCFN) alloy to which has been added one, two or three elements in different proportions, either separately or in combination, including Al, Cu, Mn, Ti, Pd, Sn, Ru, W, etc. Many different techniques have been used to characterize the structures of the resulting alloys, as well as their physical properties. Nevertheless, the understanding of why some of these alloys form simple close-packed structures and some additional intermetallic phases is still lacking. Also the mechanism behind the composition-property relationships is largely unclear.

The base CCFN alloy, even though it contains only four elements, presents the characteristics of a HEA as its diffraction pattern is apparently very simple. It has been extensively studied during the last ten years and has been reported to be single-phase and a true solid solution [6, 13, 32-34]. However, recently it was reported that CCFN alloys homogenized for a long time at high temperature are not single-phase but a coherent mixture of two solid solutions [6]. This conforms to the present study as well as to the earlier findings in [9, 35, 36] where composition fluctuations as well as fluctuations in the lattice constants as a function of position were reported in an as-cast CCFN ingot produced by arc melting and subsequent casting.

One alloy composition in the CCFN family that has been subject of limited interest is CCFN-Pd, probably because of the high cost of Pd. The structure and some physical properties have been reported in [37, 38] and it was found to be single-phase with some interesting magnetic properties. However, later work showed undoubtedly that it was at least dual-phase with a structure clearly depending on the Pd content [35, 36].

The work presented below has been performed within the AccMet European project and it is aiming at giving detailed information on the structure of the  $CCF_yN$  alloys with different Fe contents and on the  $CCFN-Pd_x$  alloys with different Pd contents by using high energy and standard X-ray as well as neutron diffraction techniques. Other papers will deal with alloy microstructure as well as with physical and magnetic properties of alloys with similar compositions and will be published in close connection to the present work [39,40].

## 2. *Experimental details*

Three different experimental diffraction techniques were used. Neutron diffraction (ND) measurements were performed on the D20 and D2B diffractometers at Institut Laue-Langevin (ILL), Grenoble (France), high-energy X-ray diffraction (HEXRD) measurements on the ID22 diffractometer at the European Synchrotron Research Facility (ESRF), Grenoble (France) and standard X-ray diffraction (XRD) with a Cobalt source at GPM, University of Rouen, France. Relevant characteristic features of the different measurements are given in table 1. All measurements were performed at ambient temperature. As all samples were found to have a pronounced texture they were rotated during the measurements, whenever possible. However, it has to be strongly emphasized that this does not completely eliminate texture effects in the recorded diffraction patterns. The penetration depth of the standard X-rays into the alloys is of the order of 1  $\mu\text{m}$  and the measurements by XRD thus give information of the structure only in a surface layer while both the ND and the HEXRD techniques yield structural information valid for the entire irradiated volume. Only a few of the ND measurements were performed on the D2B diffractometer and will be denoted ND(D2B) below, whenever referred to. Likewise, only one XRD measurement was performed with a Molybdenum source and it is denoted XRD(Mo), whenever referred to.

Ingots of  $\text{CoCrFe}_y\text{Ni}$  ( $y=0.8, 1.0$  and  $1.2$ ) and  $\text{CoCrFeNi-Pd}_x$  ( $x= 0.0, 0.5, 0.8, 1.0, 1.2, 1.5$ ) alloys (in the following denoted  $\text{CCF}_y\text{N}$  and  $\text{CCFN-Pd}_x$ , respectively) were prepared by arc melting from pure elements, each with purity higher than 99.9 wt.%, under a Ti-gettered high-purity argon atmosphere. The nominal alloy compositions are given in table 2. In order for the alloy production to be similar to most earlier studies on HEAs, the ingots were flipped and remelted several times in order to achieve melt homogeneity. It should though be noted that it has been shown in numerous works that this procedure does not ensure that the alloy melt is homogeneous [41, 42]. However, this procedure was adopted in order to avoid any ambiguity when comparing our results to those presented in the literature. Cylindrical rods with a diameter of 3 mm were subsequently prepared by suction casting the mixed alloy into a water-cooled copper mold. Four thin slices were cut from the rod and placed side by side in order to achieve a good statistical accuracy in the XRD measurements. In order to investigate their thermal stability some of the alloys were afterwards subjected to different heat and cooling treatments (see table

2). The heat treatments all lasted three hours at three different temperatures, 1100°C (T1), 700°C (T3) and 400°C (T2). T0 is the designation used for the as-cast condition in which the samples were allowed to cool in the Cu mold. The heat treated alloys were either allowed to cool in the furnace (s) or dropped into ice-water (q). All subsequent measurements were performed at ambient temperature.

### **3. Results and discussion**

#### **3.1 Results on the CC<sub>y</sub>FN alloys (y=0.8, 1.0, 1.2)**

##### **3.1.1 The structure of the CCF<sub>y</sub>N alloy in as-cast condition (T0)**

Diffraction patterns measured by the three different techniques on the CCF<sub>y</sub>N (y=1.0) alloy in as-cast condition (T0) are shown in fig. 1a. A first visual inspection of the ND and XRD patterns shows identical results and would suggest that the structure is single-phase of fcc type but on the other hand the peak shapes suggest a pronounced lattice disorder. Furthermore, no broadening of the peaks is visible in the XRD(Mo) (top curve) and the ND (2<sup>nd</sup> middle curve) patterns while in the XRD (1<sup>st</sup> middle curve) a slight symmetric broadening was observed. The effect of the different resolutions is obvious in the enlarged plot (Fig. 1b) of the (220) fcc peak. No additional phase can be detected in the alloy from the ND and XRD measurements. The asymmetry of the (220) peak in the ND measurement does indicate the presence of a distinct texture in the sample, visible due to the fact that the sample was, because of experimental conditions, kept in a fixed position during the measurements. It should however be mentioned that a peak asymmetry was seen with rotating sample on the D2B diffractometer from the same ingot. It was also found in [36] that the lattice constants derived from XRD patterns recorded from different positions in the same ingot varied slightly which was suggested to be due to the presence of a minority phase also of fcc structure but also demonstrates the pronounced texture of the CCFN alloy.

A finer structure investigation of the CCFN alloy was performed by HEXRD. The resolution in the HEXRD measurements (see table 1) is about an order of magnitude superior to the ones of the ND and XRD techniques. Thus, the ambiguity in the interpretation of the measured ND and XRD diffraction patterns could be resolved. A shape analysis of all HEXRD peaks showed that all could be decomposed into two symmetric intensity components. Several different peak shapes were tried but Gaussian functions were in all cases giving the best Goodness of Fit (GoF). Two

examples of such a breakdown of the peaks with the (hkl) Miller indices equal to (220) and (333, 511) into two components are shown in figs 2a and 2b respectively. The presence of inflection points in all measured peaks shows that the results are reliable and it definitely demonstrates that the alloy is not single-phase. Assuming an fcc structure, the lattice constants calculated from the two components of the first thirteen diffraction peaks are shown as function of  $(h^2+k^2+l^2)$  in fig. 2c. The presence of two fcc structures with slightly different lattice constants in CCFN is obvious. It can be noted that the lattice constants derived from the (200) and the (400) peaks are significantly above the average value suggesting a definite distortion of the cubic fcc structure. Such a distortion is also suggested from the variation of both peak intensities and peak widths. Unfortunately the (600) and (800) diffraction peaks do not fall within the measured angular range and thus this hypothesis can not be quantified. However, a detailed analysis of these observations is discussed in relation with simulations in a parallel paper [39]. At the present stage it is only concluded that there are clear indications that none of the two fcc lattices are true solid solutions.

In order to investigate the effect of the alloy composition on the structure further, ND and XRD measurements were performed on two  $\text{CCF}_y\text{N}$  ( $y=0.8, 1.2$ ) alloys in as-cast conditions. The diffraction patterns for all CCFN alloys as measured by ND displayed in fig. 3a are all of fcc type and they do not show within the experimental resolution any dependence of the lattice constant on Fe content. However, both non-equimolar alloys seem to contain some small additional peaks (see for example the enlarged (111) peaks in fig. 3b) that however are not numerous enough to be indexed. In HEXRD measurements on the  $\text{CCFe}_{1.2}\text{N}$  alloy, on the other hand, all diffraction peaks are asymmetric and could be decomposed into two components in the same way as was the case for the equimolar alloy. Table 3 presents the lattice constants determined for all the  $\text{CCF}_y\text{N}$  compositions by the three diffraction techniques used in this work. In all cases they have been determined from the diffraction peak positions and the estimated uncertainty due to peak anisotropies are included in the given errors. The two lattice constants derived from HEXRD data for  $y=1.2$  are slightly larger than the ones for CCFN and the difference between the two is twice as large. The extra Fe atoms have obviously promoted a more pronounced phase separation in the CCFN alloy possibly originating from increased magnetic interactions [39].

### 3.1.2 Effect of heat treatments on the structure of $\text{CCF}_y\text{N}$

In order to study their phase stability some of the as-cast CCFN alloys were subjected to different kinds of heat treatments (see table 2). The temperature values have been chosen after calorimetric investigation of the alloys. In all cases the main structure as determined from ND and XRD patterns remained generally unchanged. However, some small additional diffraction peaks (the most intense ones at  $\sim 2.5$  and  $\sim 4.5 \text{ \AA}^{-1}$ ) were observed in some measured patterns (fig. 4a). However, their intensity and their number are though too small to facilitate conclusive phase identification. Some clear effects on the diffraction patterns by the heat treatments can be clearly seen in the left part of fig. 4b. Both after T1(s) and T3(q) the lattice constant is somewhat smaller than in the as-cast one (T0) and after T1(q) treatment. The decrease might be affected by a change in alloy texture due to the heat treatment but as the same effect was observed in the  $\text{CCF}_y\text{N}$  ( $y=0.8, 1.2$ ) alloys it seems to be real. The lattice constant decreases from  $3.572 \text{ \AA}$  for as-cast CCFN to  $3.566 \text{ \AA}$  for the same alloy ingot after T1(s) treatment. The difference is within the experimental error the same for the three investigated  $\text{CCF}_y\text{N}$  alloys. This finding clearly proves the importance of considering the production technique as well as the subsequent annealing/homogenizing treatments when comparing structural and thus also physical properties of alloys nominally of the same composition. As mentioned above the difference in the thermal history of the samples can certainly in a part explain the discrepancy range in lattice constants found in the literature for the CCFN alloy. It was furthermore found that all alloy heat treatments resulted in a narrowing of the diffraction peaks and after annealing their widths were given by the experimental resolution in the ND and XRD diffraction measurements. It should though be mentioned that no CCFN alloy was investigated with HEXRD with its about 10-fold better resolution after annealing and thus nothing can be said whether its phase composition has changed.

### 3.1.3 Discussion of results on $\text{CCF}_y\text{N}$ alloys

From the HEXRD results it is concluded that the CCFN in as-cast condition is, contrary to earlier works in the literature, two-phase [6,9 and references therein]. The two lattice constants are shown in table 3 together with the ones derived from XRD and ND measurements. The agreement between the different experimental sets, taking the experimental resolution into

account, is very good. It is to be noted that, considering only the XRD and ND techniques, the results would suggest that, in accordance with most earlier works in the literature, the alloy appears to be single fcc phase and to form a perfect solid solution. However, the higher resolution HEXRD results are totally excluding this possibility. Furthermore, if carefully observed, results from other works also suggest the non solid solution as well as the non single phase state, although this was not concluded by the authors of these studies. Thus, for example, the XRD diffraction peaks shown in [34] for a CCFN alloy are clearly asymmetric in a way which might indicate the presence of two fcc phases, contrary to the interpretation given. Additional intermetallic phases have also been clearly observed in some cases. In as-cast and annealed CCFN alloys a minority Cr-rich phase slightly depleted in Co has for example been found to exist in the grain-boundaries [13, 15]. A precipitation of Cr has also been found in *ab initio* modelling [31]. Furthermore, an alloy produced by mechanical alloying has even been found to contain a minority bcc phase [43]. It can thus be concluded that not only details of the production process but also the production technique itself plays an important role in the phase composition of the alloy. Furthermore, lattice constants, spanning a range from 3.55 to 3.59 Å, reported in the literature were in many cases determined from very few measured XRD diffraction peaks. It is also important to note that XRD is a surface sensitive technique as the penetration depth is only of the order of microns. Moreover, the amount of a particular phase it is possible to detect with a certain technique is dependant on the resolution.

Recently by TEM investigations on CCFN samples that were homogenized at 1300°C (about 120 degrees below the melting point) for 1 week an onset of phase decomposition was detected [6]. The phases were found to have fcc structure and very similar unit-cell dimensions. This observation may be correlated with the HEXRD results presented above.

XRD and positron annihilation measurements on CCFN buttons produced by arc melting were reported [33]. The lattice constant was derived to 3.578 Å which is to be compared to 3.5720 Å obtained from the HEXRD measurements in the present study. It was furthermore found to decrease with annealing temperature due to a suggested defect recovery during heating. From the XRD measurements the authors concluded that the alloy was single phase and that it remained stable even after annealing 1h at 1100°C [33]. These results agree within experimental errors

with the XRD results presented above. However, none of the  $\text{CCF}_y\text{N}$  alloys investigated in the present study are single phase although having “simple” diffraction patterns”. They obviously consist of two fcc phases with close lattice parameters but the alloys appear as single phase when analyzed with lower resolution diffraction techniques (see table 1). The difference in absolute value of the derived lattice constants in the literature is due to different production techniques as well as to experimental resolution effects [36].

### **3.2 Results and discussion on CCFN-Pd<sub>x</sub> alloys**

#### **3.2.1 The structure of CCFN-Pd<sub>x</sub> alloys in as-cast condition**

Examples of measured diffraction patterns from CCFN-Pd<sub>x</sub> alloys with different Pd content in as-cast conditions from XRD, HEXRD and ND are shown in fig. 5. Measured pattern for the CCFN alloy is also shown for comparative reasons. It can immediately be noted that in all cases the main structure is of fcc type and that the unit cell increases in size with increasing Pd content [9, 35, 36]. The diffraction peak intensities vary with scattering angle in all sets of measurements in a way indicating a pronounced texture in the samples. However, it was also noted in [9, 36] that all peaks are asymmetric and can be divided into components suggesting the existence of several coexisting phases in the alloys. The suggestion is fully confirmed by the HEXRD measurements in which the experimental resolution is of the order of  $10^{-4}$ . Furthermore, fig. 6a presents the (111) diffraction peaks measured from the CCFN and CCFN-Pd<sub>x</sub> ( $x=0.5, 1.0, 1.5$ ) alloys. One peak component is sharp, resembling but somewhat wider and displaced relative to the corresponding diffraction peak in the pure CCFN alloy. One of the phase compositions identified by atom probe tomography and by microscopy in CCFN-Pd alloys is as a matter fact CoCrFeNi-rich [40]. The other peak component is considerably more displaced and it is furthermore significantly broader and asymmetric. A numerical examination based on the number of inflection points found in the differentiated peak profiles shows that all corresponding peak components can be separated into two subpeaks. Several different peak profiles were tried for this separation and all gave very closely identical results for the positions of the two subpeaks. An example of peak intensity separations assuming Gaussian shapes of the subpeaks is shown in fig. 6b. As the shape of all sharp intensity components is similar to the diffraction peaks measured for pure CCFN, it was assumed in the evaluation that the asymmetry of the peaks found for this alloy is retained when Pd atoms are incorporated in the lattice. However,

contrary to what was the case for the CCFN alloy as discussed above no decomposition into subpeaks is performed due to the absence of inflection points in the differentiated peak profiles. The lack of knowledge of exact peak shapes might make the fitting procedure non unique but it is beyond doubt that all CCFN-Pd<sub>x</sub> alloys in the composition range  $0.5 \leq x \leq 1.5$  consist of at least three phases, and considering the asymmetry of the sharpest intensity component maybe even of at least four phases. This is in full accordance with APT and EDX analyses on the same samples from which it was concluded that the alloys contain four different phases [40]. In order to determine accurately the lattice constants of the different phases the values calculated from the positions of twelve diffractions peaks for the CCFN-Pd<sub>x</sub> (x=0.5, 1.0, 1.5) alloys in as-cast conditions and measured by HEXRD are plotted as function ( $h^2+k^2+l^2$ ) in fig. 7. The difference between x=0.5 and 1.0 on one side and x=1.5 on the other side is strong indicating the large distortion of the original CCFN lattice with significant amount of included Pd atoms. The constant values for all x values on fig. 7 unambiguously show the fcc nature of the three peaks and it also yields strong support for peak analysis procedure. In the ND and the XRD measurements the experimental resolution made it possible convincingly to separate the measured peaks only into two components. Thus, the second component is to be considered as being a convolution of peaks 2 and 3 in the HEXRD measurements. The ND and XRD results are though fully compatible and those obtained from alloys in as-cast conditions are collected in table 4. They are also displayed as a function of x in fig. 8 and compared to values from [37]. However, the results obtained from XRD give somewhat different lattice constants, very probably both due to texture effects and to surface layer effects as was earlier observed [9, 35, 36]. The difference illustrates the difficulty to derive accurate lattice constants for an alloy being multi-phase, having small differences in lattice cell parameters. The values shown in table 4 are in some cases slightly different from the values given in [36] which is due to a refined analysis procedure.

It can be observed from fig. 6a that the relative amounts of the different phases that corresponds to the different peaks present in the alloys vary with Pd concentration. This is illustrated in fig. 9 that shows the average of the intensity ratios peak2/peak1 and peak3/peak1 as a function of the Pd content. The amount of the phase corresponding to peak 2 is largest close to the equimolar

composition. From microscopy investigation [40], the equimolar composition,  $x=1$ , is the one with the most distinct dendritic pattern. From the width of the peak in fig. 6b it can also be concluded that it has the smallest grain size. A similar variation of the ratios is also seen in the decomposition of the diffraction peaks measured by ND and XRD and the agreement between the different sets of data is very good. It can be concluded that the relative amounts of the different phases vary with Pd content. As the atomic compositions of the different phases are not known a full refinement will not give some relevant new information in this respect. Further discussion on the phase compositions are given in [40].

### 3.2.2 Effect of heat treatments on the structure of CCFN-Pd

Measured ND patterns for  $x=0.8$ , 1.0, and 1.2 after different heat treatments (see table 2) are shown in fig. 10. All patterns show that the main phase is fcc for all compositions and after the heat treatments. The pattern for the CCFN-Pd<sub>1.0</sub> alloy after annealing at 700°C (T3) is significantly different showing that at least one additional phase has grown in the alloy during annealing. Refinement suggests that one of these additional phases might be monoclinic. This is a slightly distorted cubic phase and can thus be considered as a metastable intermediate phase forming during the T3 annealing. The microstructure after T3 is still dendritic while it has disappeared after T1 [40]. The cell volume of this monoclinic phase happens to be almost exactly the same as the main fcc phase. However, the refinement is not fully conclusive as at least one diffraction peak in the measured pattern is not indexed. Accordingly one can conclude that an annealing of the equimolar CCFN- Pd<sub>1.0</sub> alloy at 700°C for three hours causes the alloy to decompose into at least four intermetallic phases. This conclusion is very important as 700°C is the expected temperature of use for many potential applications of High Entropy Alloys. It can furthermore be observed that for all the alloys studied the heat treatment at 1100°C (T1) resulted in a narrowing of all diffraction peaks as compared to the as-cast alloys. Moreover, their two-component nature disappeared almost completely within the resolution in both the ND and XRD measurements. This is exemplified in fig. 11 where the (311) and the (222) peaks for the CCFN-Pd<sub>0.8</sub> alloy measured by ND are shown. The same behavior was observed also for the CCFN-Pd and CCFN-Pd<sub>1.2</sub> alloys. The position of the fcc peaks after T1 is very close to the average position of the two peak components measured in as-cast condition. The measured peaks are though still slightly asymmetric indicating either a two-phase nature or a strained lattice but this is not large enough for a reliable analysis. In order to study further the stability of the

equimolar alloy the alloy that was annealed at 1100°C and ice-water cooled was again annealed at 700°C, thus T1+T3. Fig. 12 shows the measured XRD patterns compared to the ones measured in as-cast condition after all sample heat treatments. Comparing with the patterns shown in fig. 10 it is seen that the alloy structure after the second annealing is completely different. The main fcc diffraction peaks are still the most intense and their positions compare exactly with the ones measured from the as-cast alloy, i.e. corresponding to a lattice constant of 3.660 Å. However, on each side of these two well resolved peaks can now be seen, the positions of which can be refined to correspond to two fcc structures, one with  $a=3.615\text{Å}$  and one with  $a=3.743\text{Å}$ . The small lattice constant does not correspond to any binary compound of the alloy containing elements while the largest one closely corresponds to the CoPd alloy, 3.75Å. The calculated lattice constant for the ordered FeCrNi alloy has been found to 3.562Å [44] in fair agreement with the  $a=3.615\text{Å}$  value given above [39]. The T1+T3 pattern also shows some faint indications of further diffraction peaks but these are too few to be used for a structure identification. The patterns presented in fig. 10 to 12 unequivocally show that the phase content of the CCFNPd alloy after heat treatment T1 is different from the phase content in as-cast condition (T0) and that the detailed structural evolution during subsequent heatings from T0 and from T1 is significantly different. This fact has a pronounced influence of the physical properties [39,40].

#### **4. Conclusions**

It was concluded from the diffraction patterns measured with the highest experimental resolution, i.e. by high-energy X-rays, that the CoCrFeyNi ( $y=0.8$  and  $1.2$ ) alloy in as-cast condition is, contrary what is claimed in the literature, not single-phase but consists of at least two different phases both of fcc type. The difference in lattice constant between the two phases is close to  $0.001\text{Å}$ . Diffraction patterns measured by X-ray and neutron diffraction have shown that the structure of the alloy is not obviously affected by 3 hours heat treatments up to 1100°C. Changing the amount of Fe has no drastic effect on alloy structure.

The structure of the high-entropy CoCrFeNi-Pd<sub>x</sub> ( $x= 0.0, 0.5, 0.8, 1.0, 1.2, 1.5$ ) alloys in as-cast conditions and after heat treatments has been characterized by using three different kinds of radiation, high-energy X-rays, standard X-rays and neutrons. The three diffraction techniques

have experimental resolutions varying from about 0.03 to about 1%. All Pd containing alloys have been found to consist of at least four different phases, all being of fcc type. The lattice constants for all phases increase with Pd content which indicates that Pd atoms have been incorporated in the CoCrFeNi lattice. The relative amounts of the different phases are found to depend on Pd concentration. Heat treatments during three hours at different temperatures have a significant effect on the alloy phase composition.

Accordingly and contrary to the standard definition found in the literature, the CoCrFe<sub>y</sub>Ni-Pd<sub>x</sub> HEAs investigated in the present study are not single phase but have “simple” diffraction pattern, e.g. one or several fcc-type, bcc-type, or hcp-type of close lattice distances. Thus a more appropriate definition of HEA might be that “HEAs are multicomponent alloys presenting simple diffraction patterns of fcc, hcp or bcc type.

## References

1. Y. Zhang, T.T. Zuo, Z. Tang, M.C. Gao, K.A. Dahmen, P.K. Liaw, Z.P.Lu, Microstructures and properties of high-entropy alloys, *Prog. Mater. Sci.* 61 (2014) 1-93.
2. M.-H. Tsai, J.-W. Yeh, High-entropy alloys: A critical review, *Mater. Res. Lett.* 2 (2014) 107-123.
3. B. Cantor, I.T.H. Chang, P. Knight, A.J.B. Vincent, Microstructural development in equiatomic multicomponent alloys, *Mater. Sci. Eng. A* 375-377 (2004) 213-218.
4. B. Cantor, Multicomponent and high entropy alloys, *Entropy* 16 (2014) 4749-4768.
5. O.N. Senkov, J.D. Miller, D.B. Miracle, C. Woodward, Accelerated exploration of multi-principal element alloys for structural applications, *CALPHAD* 50 (2015) 32-48.
6. R. Kozak, A. Sologubenko, W. Steurer, Single-phase high-entropy alloys – an overview, *Z. Kristallogr.* 230 (2015) 55-68.
7. J.-W. Yeh, S.-K. Chen, S.-J. Lin, J.-Y. Gan, T.-S. Chin, T.-T. Shun, C.-H. Tsau, S.-Y. Chang, Nanostructured high-entropy alloys with multiple principal elements: Novel alloy design concepts and outcomes, *Adv. Eng. Mater.* 6 (2004) 299-303.
8. L.J. Santodonato, Y. Zhang, M. Feygenson, C.M. Parish, M.C. Gao, R.J. Weber, J.C. Neufeind, Z. Tang, P.K. Liaw, Deviation from high-entropy configurations in the atomic distributions of a multi-principal-element alloy, *Nature Com.* 6 (2015) 5964.
9. J. Cornide, U. Dahlborg, Z. Leong, L. Asensio Dominguez, J. Juraszek, S. Jouen, T. Hansen, R. Wunderlich, S. Chambreland, I. Todd, R. Goodall, M. Calvo-Dahlborg, Structure and properties of some CoCrFeNi-based high Entropy alloys, *The Minerals, Metals & Materials Society 2015, TMS2015, Supplemental Proceedings*, John Wiley & Sons, Inc., Hoboken, NJ, USA. DOI: 10.1002/9781119093466.ch139.
10. D.B. Miracle, J.D. Miller, O.N. Senkov, C. Woodward, M.D. Uchic, J. Tiley, Exploration and development of high entropy alloys for structural applications, *Entropy* 16 (2014) 494-525.
11. Z.P. Lu, H. Wang, M.W. Chen, I. Baker, J.W. Yeh, C.T. Liu, T.G. Nieh, An assessment on the future development of high-entropy alloys: Summary from a recent workshop, *Intermetallics* 66 (2015) 67-76.
12. S. Guo 2013, C. Ng, J. Lu, C.T. Liu, Effect of valence electron concentration on stability of fcc or bcc phases in high entropy alloys, *J. Appl. Phys.* 109 (2011) 103505(5).

13. S. Guo, C. Ng, Z.J. Wang, C.T. Liu, Solid solutioning in equiatomic alloys: Limit set by topological instability, *J. Alloys Comp.* 583 (2014) 410-413.
14. F. Otto, Y. Yang, H. Bei, E.P. George, Relative effects of enthalpy and entropy on the phase stability of equiatomic high-entropy alloys, *Acta Mater.* 61 (2013) 2628-2638.
15. A.K. Singh, A. Subramaniam, On the formation of disordered solid solutions in multi-component alloys, *J. Alloys Comp.* 587 (2014) 113-119.
16. A.K. Singh, N. Kumar, A. Dwivedi, A. Subramaniam, A geometrical parameter for the formation of disordered solid solutions in multi-component alloys, *Intermetallics* 53 (2014) 112-119.
17. M.G. Poletti, L. Battezzati, Electronic and thermodynamic criteria for the occurrence of high entropy alloys in metallic systems, *Acta Mater.* 75 (2014) 297-306.
18. Y.F. Ye, Q. Wang, J. Lu, C.T. Liu, Y. Yang, Design of high entropy alloys: A single-parameter thermodynamic rule, *Scripta Mater.* 104 (2015) 53-55.
19. Y.F. Ye, C.T. Liu, Y. Yang, A geometric model for intrinsic residual strain and phase stability in high entropy alloys, *Acta Mater.* 94 (2015) 152-161.
20. Yiping Lu, Yong Dong, Li Jiang, Tongmin Wang, Tingju. Li, Yong Zhang, A criterion for topological close-packed phase formation in high entropy alloys, *Entropy* 17 (2015) 2355-2366.
21. O.N. Senkov, D.B. Miracle, A new thermodynamic parameter to predict formation of solid solution or intermetallic phases in high entropy alloys, *J. Alloys Compd.* 658 (2016) 603-607.
22. Zhijun Wang, Weifeng Qiu, Yong Yang, C.T. Liu, Atomic-size and lattice-distortion effects in newly developed high-entropy alloys with multiple principal elements, *Intermetallics* 64 (2015) 63-69.
23. I. Toda-Caraballo, E.I. Galindo-Nava, P.E.J. Rivera-Diaz-del-Castillo, Unravelling the materials genome: Symmetry relationships in alloy properties, *J. Alloys Comp.* 566 (2013) 217-228.
24. I. Toda-Caraballo, J.S. Wrobel, S.I. Dudarev, D. Nguyen-Manh and P.E.J. Rivera-Diaz-del-Castillo. Interatomic spacing distribution in multicomponent alloys, *Acta Mater.* 97 (2015) 156-169.
25. L. Asensio Dominguez, R. Goodall, I. Todd, Prediction and validation of quaternary high entropy alloys using statistical approaches, *Mat. Sci. Techn.* 31 (2015) 1201-1206.

26. R. Raghavan, K.C. Hari Kumar, B.S. Murty, Analysis of phase formation in multi-component alloys, *J. Alloys Comp.* 544 (2012) 152-158.
27. M.C. Gao, D.E. Alman, Searching for next single-phase high-entropy alloy compositions, *Entropy* 15 (2013) 4504-4519.
28. F. Zhang, C. Zhang, S.L. Chen, J. Zhu, W.S. Cao, U.R. Kattner, An understanding of high entropy alloys from phase diagram calculations, *CALPHAD* 45 (2014) 1-10.
29. M.C. Tropicovsky, J.R. Morris, P.R.C. Kent, A.R. Lupini, G.M. Stocks, Criteria for predicting the formation of single-phase high-entropy alloys, *Phys. Rev. X* 5 (2015) 011041(6).
30. F. Tian, L.K. Varga, N. Chen, L. Delczeg, L. Vitos, Ab initio investigation of high-entropy alloys of 3d elements, *Phys. Rev. B* 87 (2013) 075144(8).
31. S.C. Middleburgh, D.M. King, G.R. Lumpkin, M. Cortie, L. Edwards, Segregation and migration of species in the CrCoFeNi high entropy alloy, *J. Alloys Comp.* 599 (2014) 179-182.
32. Z. Wu, H. Bei, F. Otto, G.M. Pharr, E.P. George, Recovery, recrystallization, grain growth, and phase stability of a family of FCC-structured multi-component equiatomic solid solution alloys, *Intermetallics* 46 (2014) 131-140.
33. S. Abhaya, R. Rajaraman, S. Klavathi, G. Amarendra, Positron annihilation studies on FeCrCoNi high entropy alloy, *J. Alloys Comp.* 620 (2015) 277-282.
34. M.S. Lucas, G.B. Wilks, L. Mauger, J.A. Muñoz, O.N. Senkov, E. Michel, J. Horwath, S.L. Semiatin, M.B. Stone, D.L. Abernathy, E. Karapetrova, Absence of long-range chemical ordering in equimolar FeCoCrNi, *Appl. Phys. Lett.* 100 (2012) 251907(4).
35. J. Cornide, M. Calvo-Dahlborg, S. Chambreland, L. Asensio Dominguez, Z. Leong, U. Dahlborg, A. Cunliffe, R. Goodall, I. Todd, Combined Atom Probe Tomography and TEM investigations of CoCrFeNi, CoCrFeNi-Pdx ( $x=0.5, 1.0, 1.5$ ) and CoCrFeNi-Sn, *Acta Phys. Polonica A* 128 (2015) 557-560.
36. U. Dahlborg, J. Cornide, M. Calvo-Dahlborg, T.C. Hansen, Z. Leong, L. Asensio Dominguez, S. Chambreland, A. Cunliffe, R. Goodall, I. Todd, Crystalline structures of some High Entropy Alloys obtained by Neutron and X-ray diffraction, *Acta. Phys. Polonica* 128 (2015) 552-556.
37. M.S. Lucas, L. Mauger, J.A. Muñoz, Y. Xiao, A.O. Sheets, S.L. Semiatin, J. Horwath, Z. Turgut, Magnetic and vibrational properties of high-entropy alloys, *J. Appl. Phys.* 109 (2011) 07E307(3).

38. M.S. Lucas, D. Belyea, C. Bauer, N. Bryant, E. Michel, Z. Turgut, S.O. Leontsev, J. Horwath, S.L. Semiatin, M.E. McHenry, C.W. Miller, Thermomagnetic analysis of FeCoCr<sub>x</sub>Ni alloys: Magnetic entropy of high-entropy alloys, *J. Appl. Phys.* 113 (2013) 17A923(3).
39. M. Calvo-Dahlborg, J. Cornide, D. Nguyen-Manh, J.S. Wróbel, J. Tobola, J. Juraszek, S. Jouen, U. Dahlborg, Effect of Pd on structural and magnetic properties of CoCrFe<sub>y</sub>Ni-Pd<sub>x</sub> alloys, for x between 0 and 1.5 and y=0.8, 1.0 and 1.2, to be submitted.
40. Distribution of Pd atoms in CoCrFeNi-Pd<sub>x</sub> High Entropy Alloys, J. Cornide, G.D. Hatton, M. Calvo-Dahlborg, Z. Leong, S. Chambreland, U. Dahlborg, A. Fones, R. Goodall, to be submitted.
41. I.G. Brodova, P.S. Popel, G.I. Eskin, *Liquid Metal Processing: Applications to Aluminium Alloy Production*, Advances in Metallic Alloys, J.N. Fridlyander, D.G. Eskin (Eds.), Taylor & Francis, London, 2002.
42. P.S. Popel, M. Calvo-Dahlborg, U. Dahlborg, Metastable microheterogeneity of melts in eutectic and monotectic systems and its influence on the solidified alloy, *J. Non-Cryst. Solids* 353 (2007) 3243-3253.
43. S. Praveen, B.S. Murty, R.S. Kottada, Alloying behavior in multi-component AlCoCrCuFe and NiCoCrCuFe high entropy alloys, *Mater. Sci. Eng. A* 534 (2012) 83-89.
44. J.S. Wrobel, D. Ngyuen-Manh, M.Y. Lavrentiev, M. Muzyk, S.L. Dudarev, Phase stability of ternary fcc and bcc Fe-Cr-Ni alloys, *Phys. Rev. B* 91 (2015) 024108(31).

## Acknowledgement

The authors are thankful to Institute Laue-Langevin, Grenoble, France, for awarding beam-time on the D20 and D2B diffractometers at the ILL reactor. The present work has been carried out within the FP7 European project AccMet, Contract NMP4-LA-2011-263206.

	Neutron diffraction (ND) (ILL)		High-energy X- ray diffraction (HEXRD) (ESRF) ID22	Standard X-ray diffraction (XRD) (GPM)
	D20	D2B		
Wavelength of incident radiation (Å)	1.123	1.595	0.400913	1.78897, 1.79285
Resolution ( $\Delta Q/Q$ ) at $Q=3 \text{ \AA}^{-1}$ (%)	~1	~0.2	~ 0.03	~0.2
Measurement geometry	T (fixed sample)	T (rotating sample)	T (rotating sample)	R (fixed sample)

Table 1. Experimental parameters for the different diffraction measurements. The wavevector  $Q$  is given by  $Q=4\pi/\lambda\sin(\theta)$  where  $\lambda$  is the wavelength of the incident radiation and  $2\theta$  the scattering angle. T denotes transmission geometry and R reflection, respectively.

CCF <sub>y</sub> NPd <sub>x</sub>		ND (ILL)		HEXRD (ESRF)	XRD (GPM)
Nominal alloy composition		D20	D2B		
y	x				
0.8	0	Co <sub>26.3</sub> Cr <sub>26.3</sub> Fe <sub>21.1</sub> Ni <sub>26.3</sub>	T0, T1(q), T1 (s), T2(q), T3(q)		
1.0	0	Co <sub>25</sub> Cr <sub>25</sub> Fe <sub>25</sub> Ni <sub>25</sub>	T0, T1(q), T1(s), T2(q), T3(q)	T0	T0, T1(q), T1(s), T3(q), T3(q), T1(q)+T3(q)
	0.5	Co <sub>22.2</sub> Cr <sub>22.2</sub> Fe <sub>22.2</sub> Ni <sub>22.2</sub> Pd <sub>11.1</sub>		T0	T0
	0.8	Co <sub>20.8</sub> Cr <sub>20.8</sub> Fe <sub>20.8</sub> Ni <sub>20.8</sub> Pd <sub>16.7</sub>	T0, T1(q), T3(q)		
	1.0	Co <sub>20</sub> Cr <sub>20</sub> Fe <sub>20</sub> Ni <sub>20</sub> Pd <sub>20</sub>	T0, T1(q), T3(q)	T1(q), T1(s)	T0, T1(q), T3(q), T1(q)+T3(q)
	1.2	Co <sub>19.2</sub> Cr <sub>19.2</sub> Fe <sub>19.2</sub> Ni <sub>19.2</sub> Pd <sub>23.1</sub>	T0, T1(q), T3(q)		
	1.5	Co <sub>18.2</sub> Cr <sub>18.2</sub> Fe <sub>18.2</sub> Ni <sub>18.2</sub> Pd <sub>27.3</sub>		T0	T0
1.2	0	Co <sub>23.8</sub> Cr <sub>23.8</sub> Fe <sub>28.6</sub> Ni <sub>23.8</sub>	T0, T1(q), T3(q)	T0	

Table 2. List of alloys in different conditions investigated by the experimental techniques used in the present work. (T0) corresponds to an alloy in as-cast condition allowed to cool in the Cu mold while (T1), (T2) and (T3) denotes the temperatures 1100°C, 400°C, and 700°C, respectively, at which the alloy was kept during 3 hours. (q) indicates that the alloy after

annealing has been dropped into ice water and (s) that the alloy was allowed to cool in the furnace. All measurements were performed at ambient temperature.

Alloy	High-energy X-rays (HEXRD)		Standard X-rays (XRD)	Neutrons (ND)
	Peak 1	Peak 2		
CCF <sub>0.8</sub> N	-	-	3.573(2)	3.570(3)
CCF <sub>1.0</sub> N	3.5721(1)	3.5733(3)	3.575(3)	3.580(3)
CCF <sub>1.2</sub> N	3.5749(2)	3.5770(5)	3.572(3)	3.575(3)

Table 3. Determined fcc lattice constants of investigated CCF<sub>y</sub>N (y=0.8, 1.0, 1.2) alloys in as-cast conditions (T0). Peak 1 and peak 2 correspond to the two intensity components in fig. 2. The numbers within brackets indicates the error in the last digit as obtained from a realistic refinement.

Alloy	High-energy X-rays (HEXRD)			Standard X-rays (XRD)		Neutrons (ND)	
	Peak 1	Peak 2	Peak 3	Peak 1	Peak 2	Peak 1	Peak 2
CCFN-Pd <sub>0.5</sub>	3.6201(3)	3.6327(6)	3.6437(8)	3.631(3)	3.643(5)	-	-
CCFN-Pd <sub>0.8</sub>	-	-	-	-	-	3.634(2)	3.656(3)
CCFN-Pd <sub>1.0</sub>	3.6595(3)	3.6752(7)	3.6871(6)	3.662(3)	3.678(5)	3.656(2)	3.673(3)
CCFN-Pd <sub>1.2</sub>	-	-	-	-	-	3.668(3)	3.686(3)
CCFN-Pd <sub>1.5</sub>	3.699(1)	3.705(1)	3.710(1)	3.705(3)	3.721(5)	-	-

Table 4. Determined fcc lattice constants of investigated CCFN-Pd<sub>x</sub> (x=0.5, 0.8, 1.0, 1.2, 1.5) alloys in as-cast conditions (T0). Peak 1, peak 2 and peak 3 correspond to the two and three intensity components identified with similar method as in fig. 6b. The numbers within brackets indicates the error in the last digit as obtained from a realistic refinement.

### Figure captions

Fig. 1 (a) Measured diffraction patterns for a CCFN alloy by different experimental techniques. (b) The fcc (220) peak on an enlarged scale. Patterns are measured by HEXRD (bottom curve), XRD (1<sup>st</sup> middle curve), ND (2<sup>nd</sup> middle curve) and XRD(Mo) (top curve). The corresponding Miller indices are shown in a).

Fig. 2 (a) The fcc (220) and (b) the fcc (333, 511) peaks in the diffraction pattern measured by high-energy X-rays divided into two components. (c) Lattice constants derived from the two components of every diffraction peak assuming an fcc lattice.

Fig. 3 (a) ND patterns measured from CCF<sub>0.8</sub>N (bottom curve), CCFN (middle curve), and CCF<sub>1.2</sub>N (top curve). (b) The (111) fcc peak at an enlarged scale. The corresponding Miller indices are shown in a). The arrow in b) points to an unindexed peak.

Fig. 4 (a) Measured neutron diffraction patterns from CCFN after different heat treatments. Notations from bottom to top: (T0) in as-cast condition. (T1(q)) after 3 hours at 1100°C and cooled in ice-water. (T1(s)) after 3 hours at 1100°C and cooled in furnace, (T3(q)) after 3 hours at 700°C and cooled in ice water. The vertical bars correspond to diffraction peaks for an fcc lattice with  $a=3.572 \text{ \AA}$ . The corresponding Miller indices are shown. (b) The fcc (311) peaks at an enlarged scale.

Fig. 5 Diffraction patterns obtained by different experimental techniques from CCFN-Pd<sub>x</sub> alloys of several Pd contents. a) HEXRD, b) XRD and c) ND. In a) and b) the patterns correspond to, from below,  $x=0, 0.5, 1.0, 1.5$  and in c) to  $x=0.0, 0.8, 1.0, 1.2$ . The corresponding Miller indices are located at the positions of the diffraction peaks for the CCFN alloy.

Fig. 6 (a) The (111) diffraction peaks for CCFN-Pd<sub>x</sub> ( $x=0, 0.5, 1.0, 1.5$ ) alloys as measured by HEXRD. (b) decomposition of the (111) peak for the CCFN-Pd<sub>1.0</sub> alloy.

Fig. 7 Lattice constants for the three peak components according to figure 5 derived separately from all diffraction peak with Miller indices (hkl) assuming the alloys contain only fcc structures for a) CCFN-Pd<sub>0.5</sub>, b) CCFN-Pd<sub>1.0</sub>, and c) CCFN-Pd<sub>1.5</sub>.

Fig. 8 Derived average lattice constants corresponding to first two diffraction peaks for CCFN-Pd<sub>x</sub> alloys as a function of x, determined by HEXRD (squares), ND (circles), and XRD (triangles). The crosses refer to values reported in [38].

Fig. 9 Ratio between measured intensities of the peaks defined in fig. 5 for CCFN-Pd<sub>x</sub> alloys as function of x, determined by HEXRD (squares), ND (circles) and XRD (triangles). Full symbols correspond to the ratio peak2/peak1, open symbols to peak3/peak1 in fig. 5.

Fig.10 Measured ND patterns for a) CCFN-Pd<sub>0.8</sub>, b) CCFN-Pd<sub>1.0</sub>, and c) CCFN-Pd<sub>1.2</sub> after different heat treatments. From below T0, T1(q), T3(q). The vertical bars correspond to diffraction peaks for an fcc lattices with lattice constants given in table 4. The corresponding Miller indices are shown.

Fig 11 The fcc (331) and (420) peaks as measured by ND from the CCFN-Pd<sub>0.8</sub> alloy after different heat treatments. From below T0, T1(q), T3(q).

Fig.12 (a) Measured XRD patterns CCFN-Pd alloys after different heat treatments. The curves correspond to, from below, T0, T1(q), T3(q), T1(q)+T3(q) conditions. The Miller indices are shown. (b) the fcc (111) and (200) peaks on an enlarged scale. The order of the curves is the same as in (a). Vertical bars correspond to fcc lattices with, from below, lattice distances  $a=3.615, 3.66, \text{ and } 3.74\text{\AA}$ , respectively.

## Highlights

As-cast CoCrFeNi is not single-phase but made of at least two different fcc phases.

All investigated CoCrFeNiPd<sub>x</sub> alloys consist of at least three different fcc phases.

Standard heat treatments have a significant effect on the alloy phase composition.

**Figure**  
Click here to download high resolution image

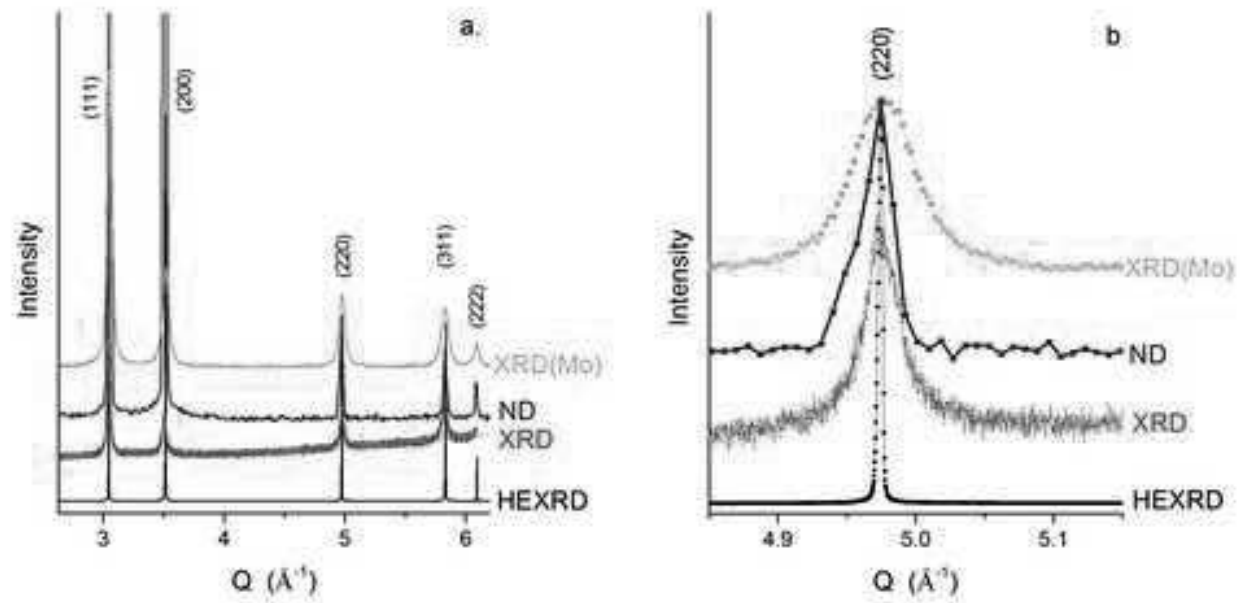


Figure  
Click here to download high resolution image

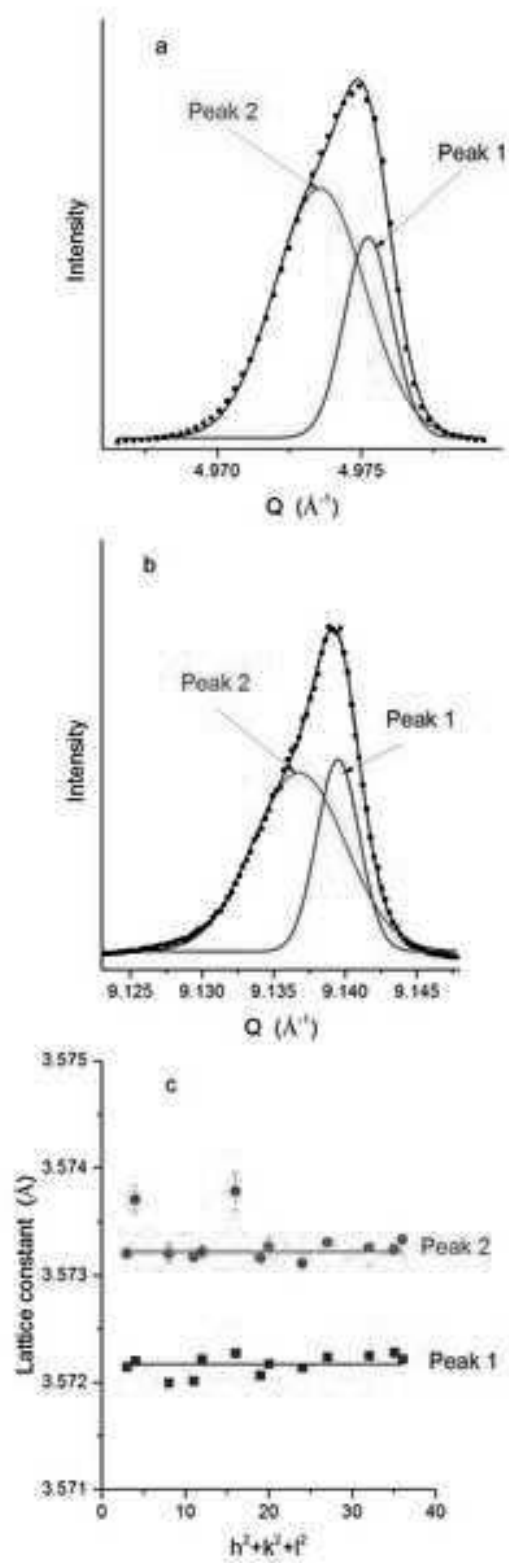


Figure  
Click here to download high resolution image

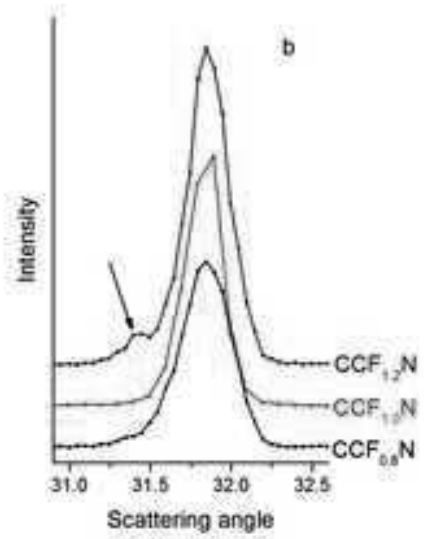
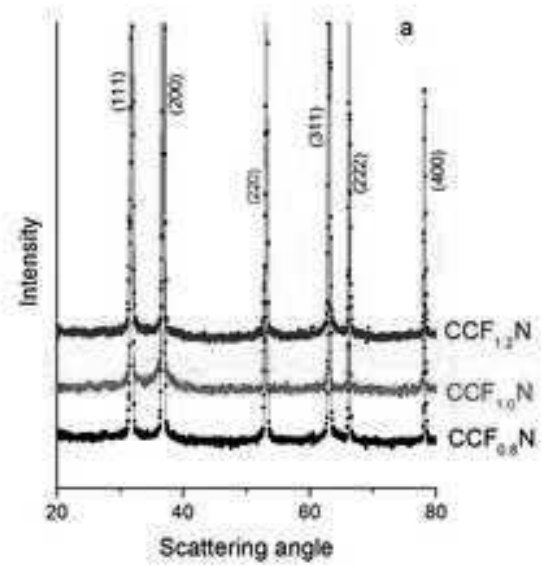


Figure  
Click here to download high resolution image

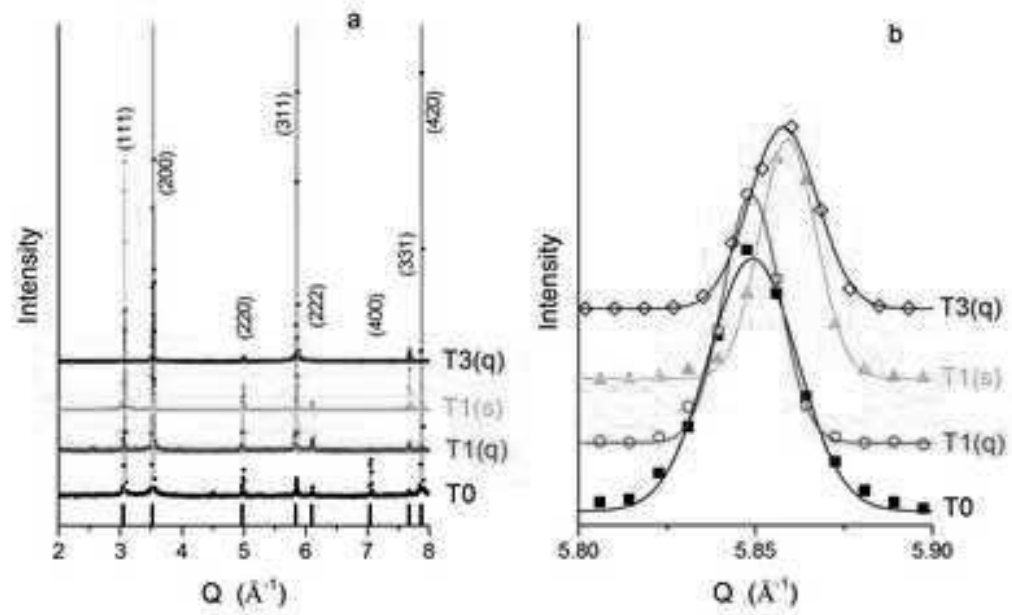


Figure  
Click here to download high resolution image

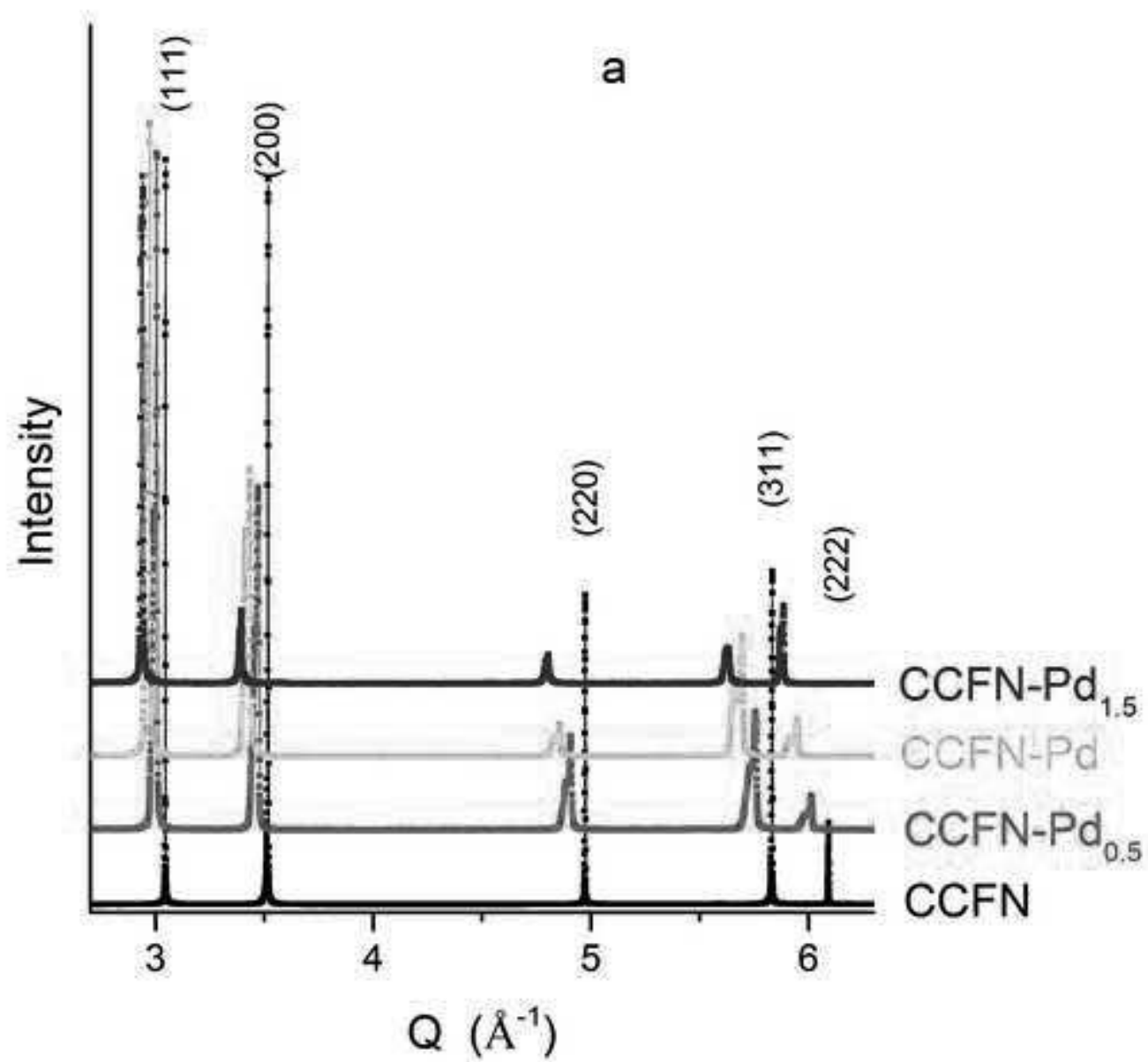


Figure  
Click here to download high resolution image

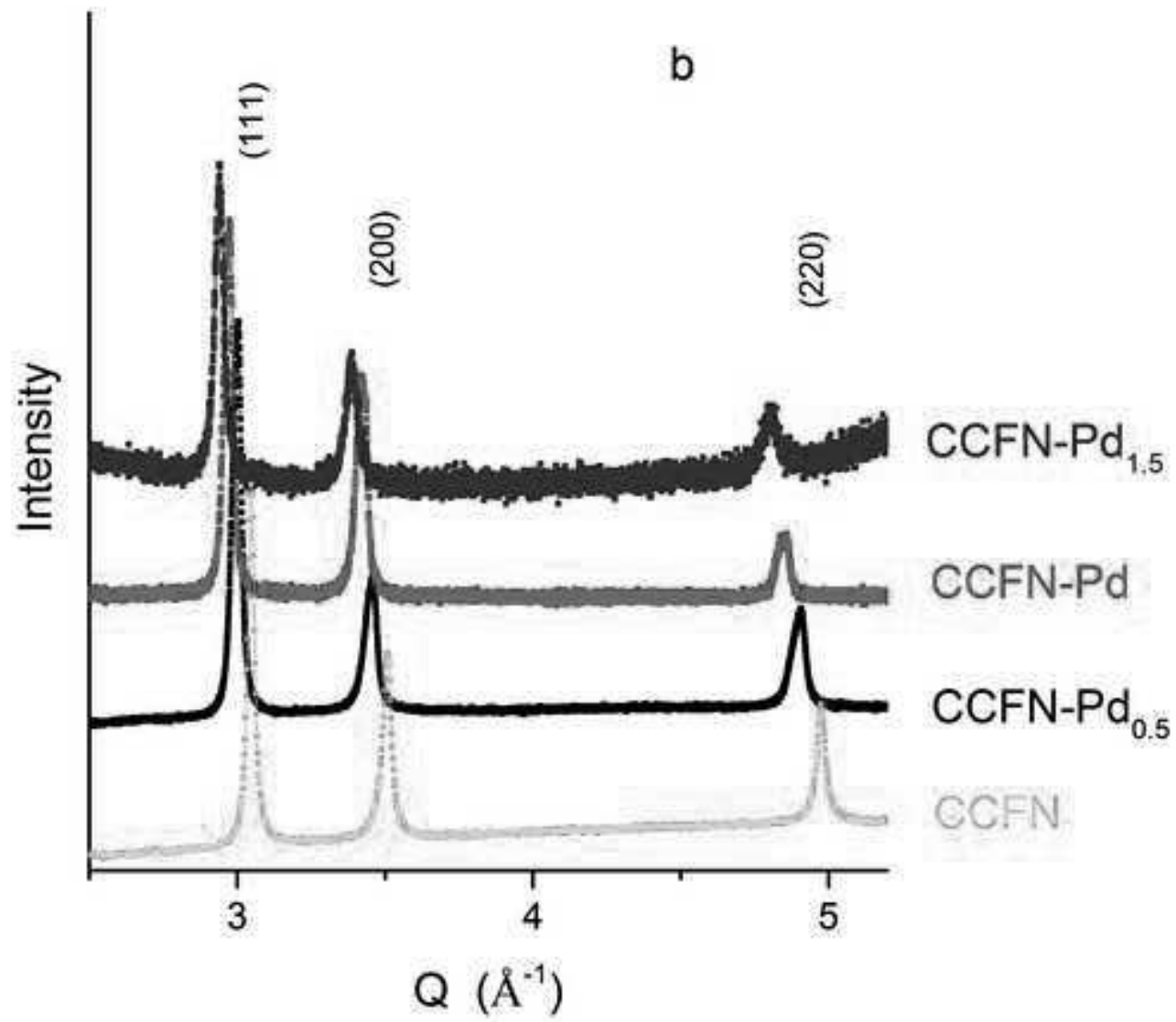


Figure  
Click here to download high resolution image

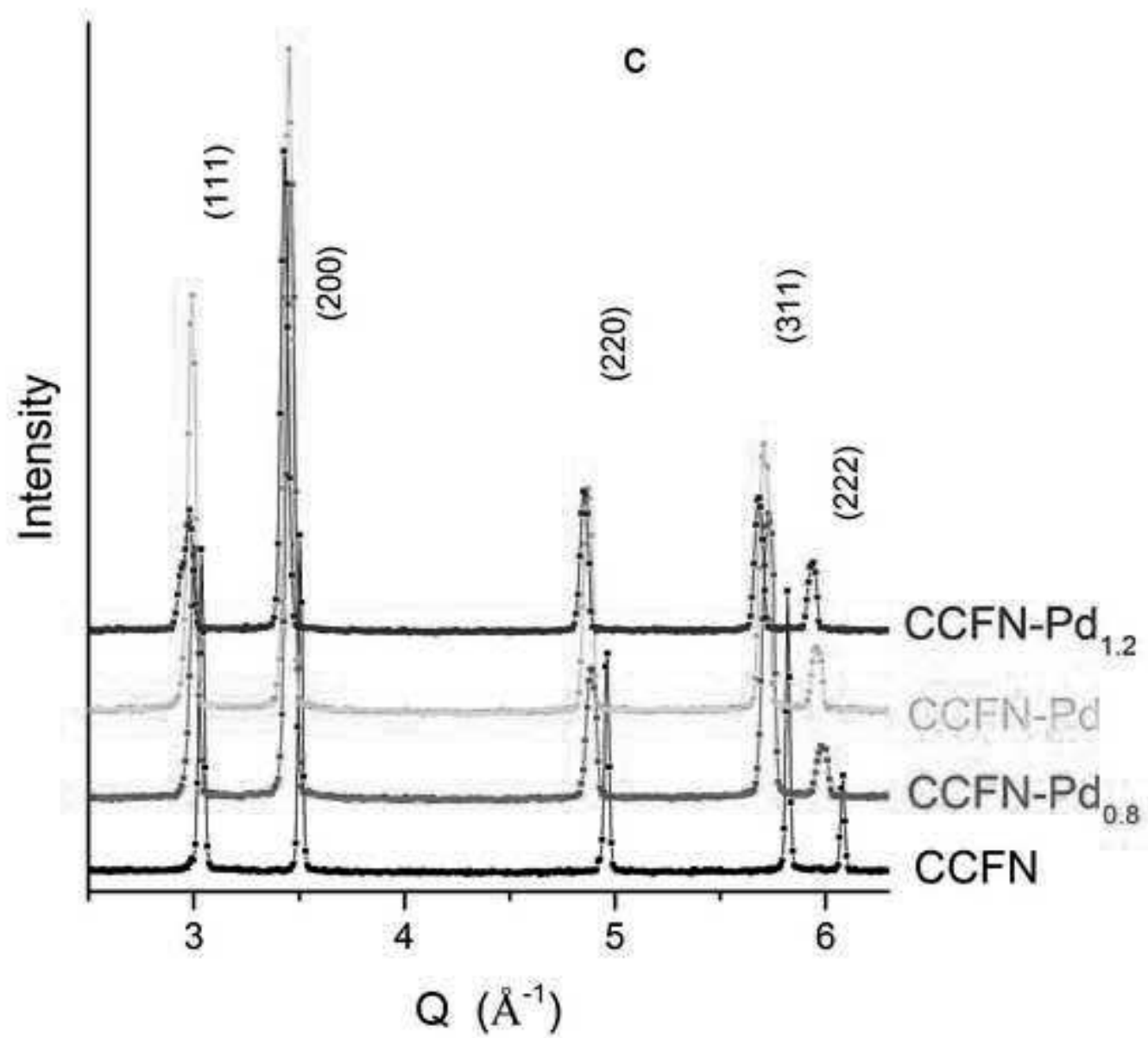


Figure  
Click here to download high resolution image

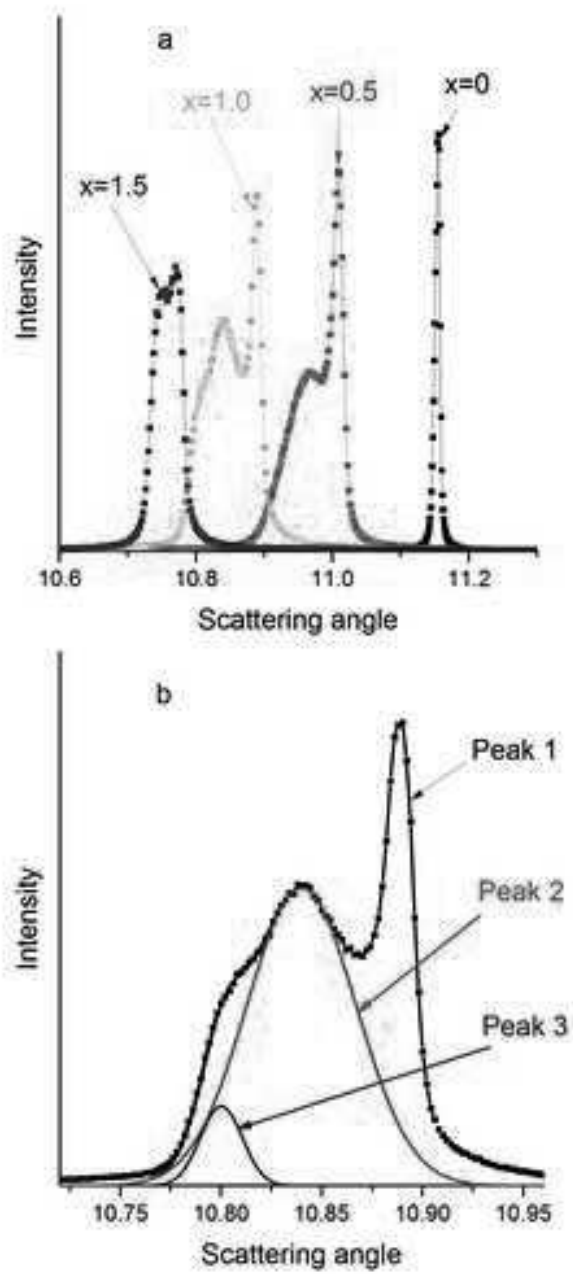
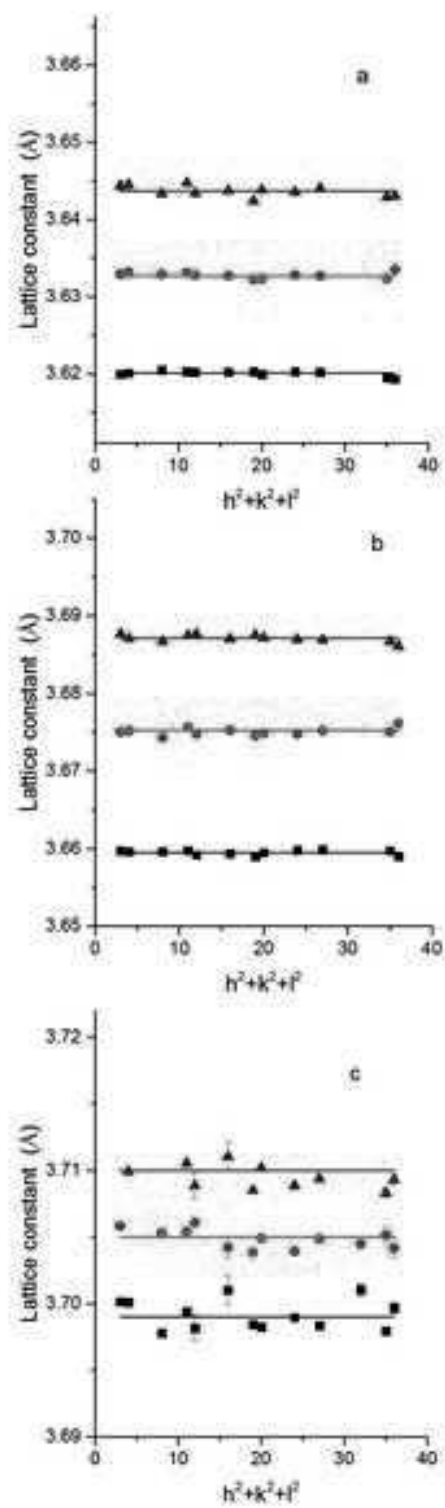


Figure  
Click here to download high resolution image



# Figure

[Click here to download high resolution image](#)

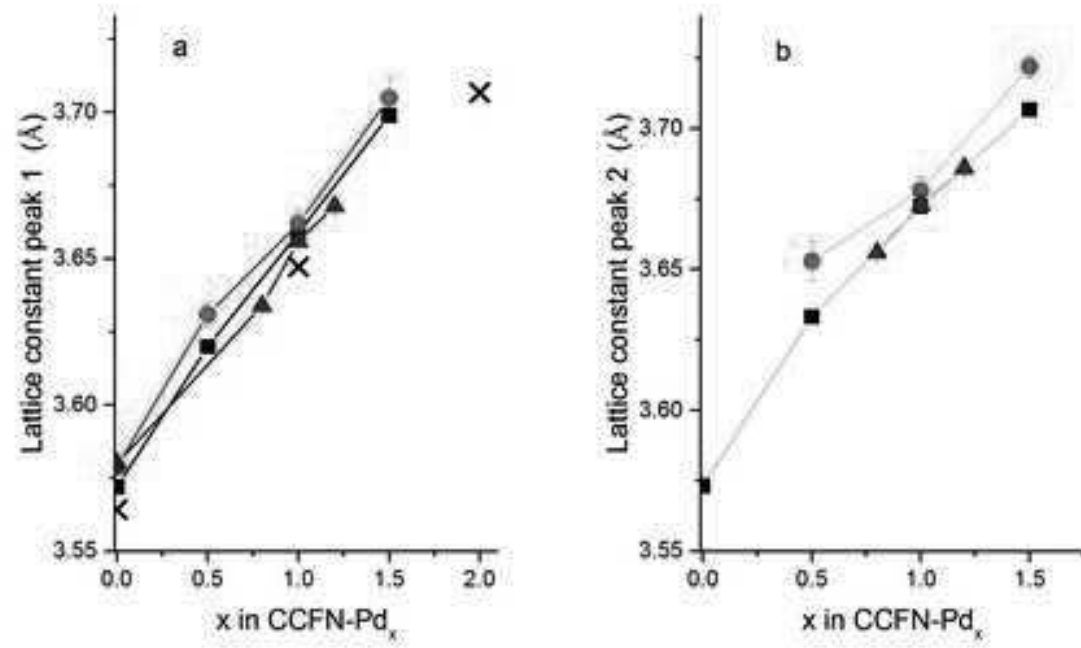


Figure  
Click here to download high resolution image

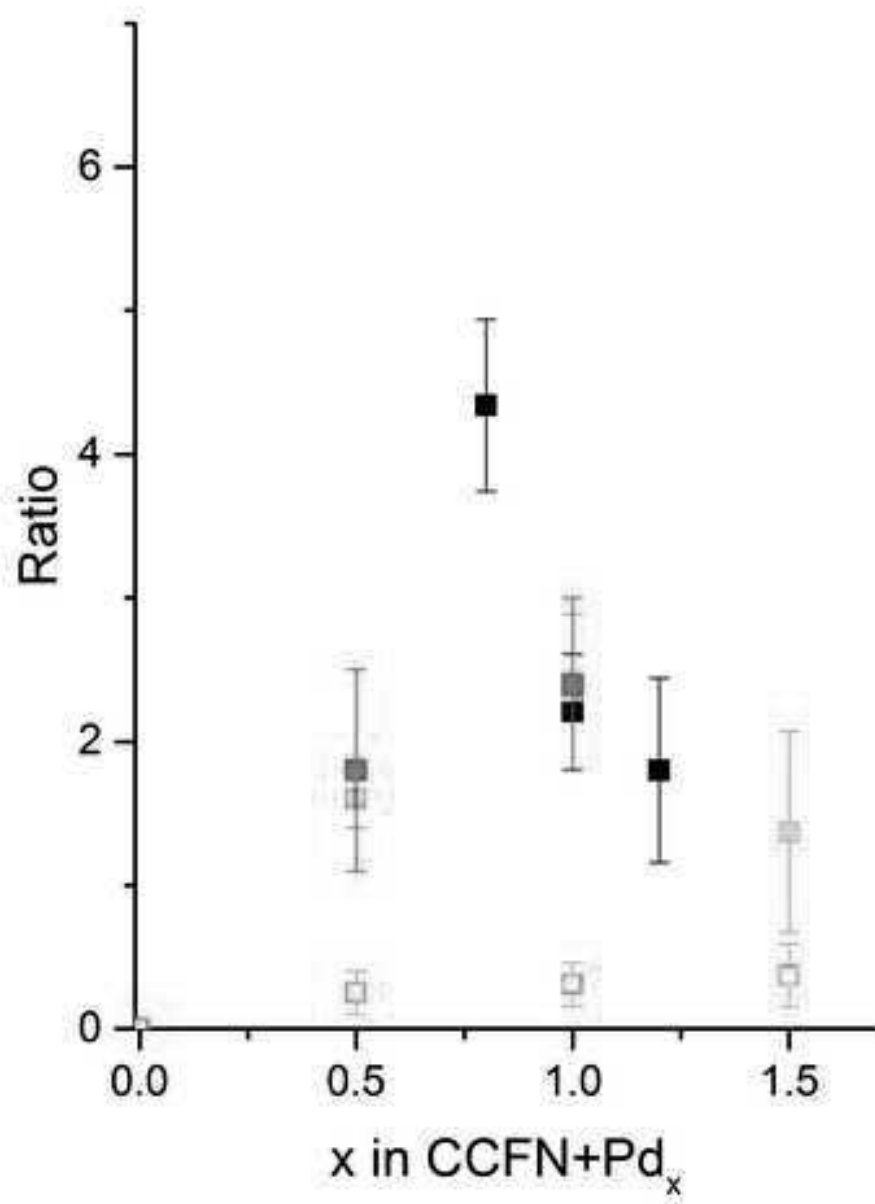


Figure  
Click here to download high resolution image

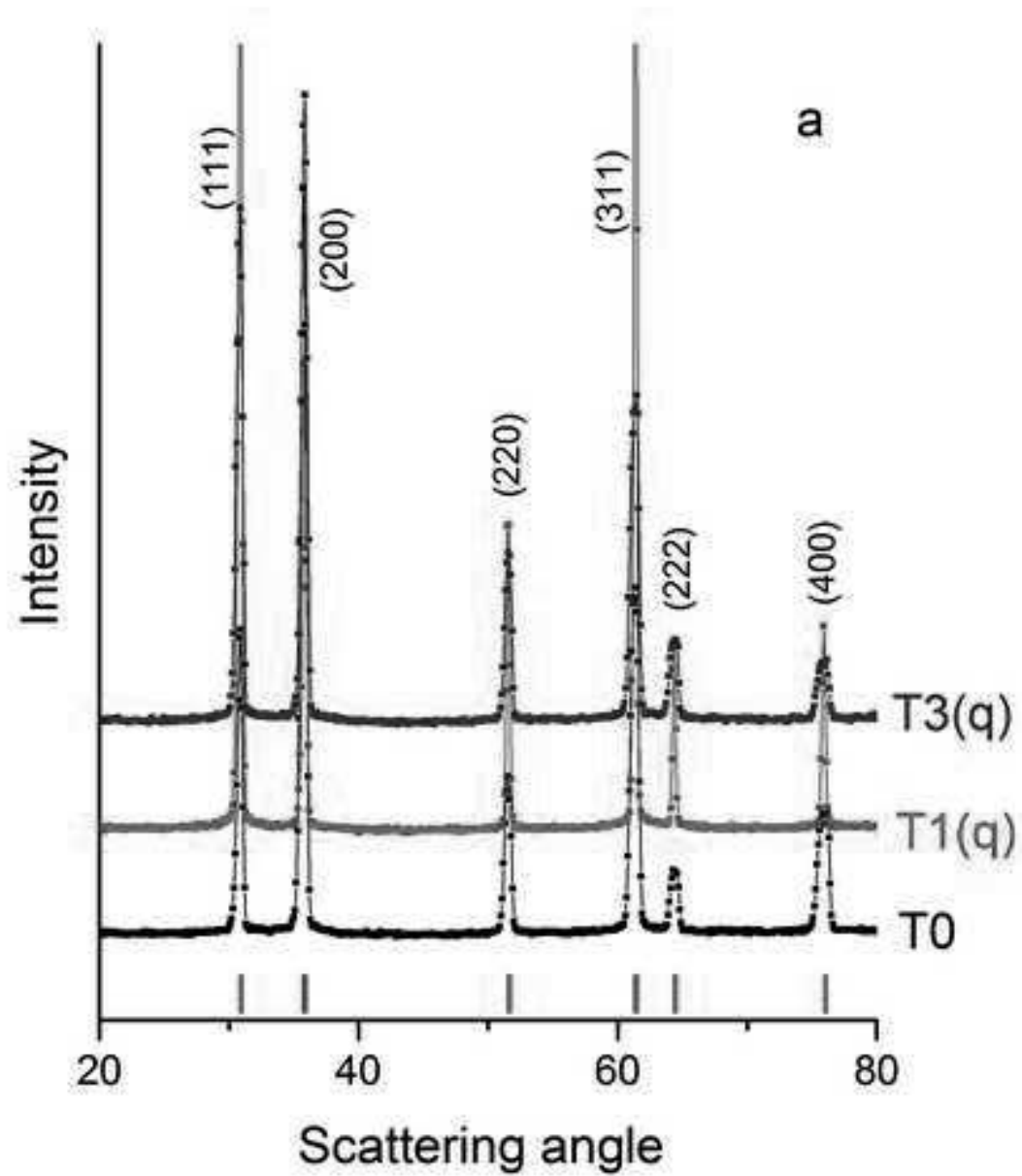


Figure  
Click here to download high resolution image

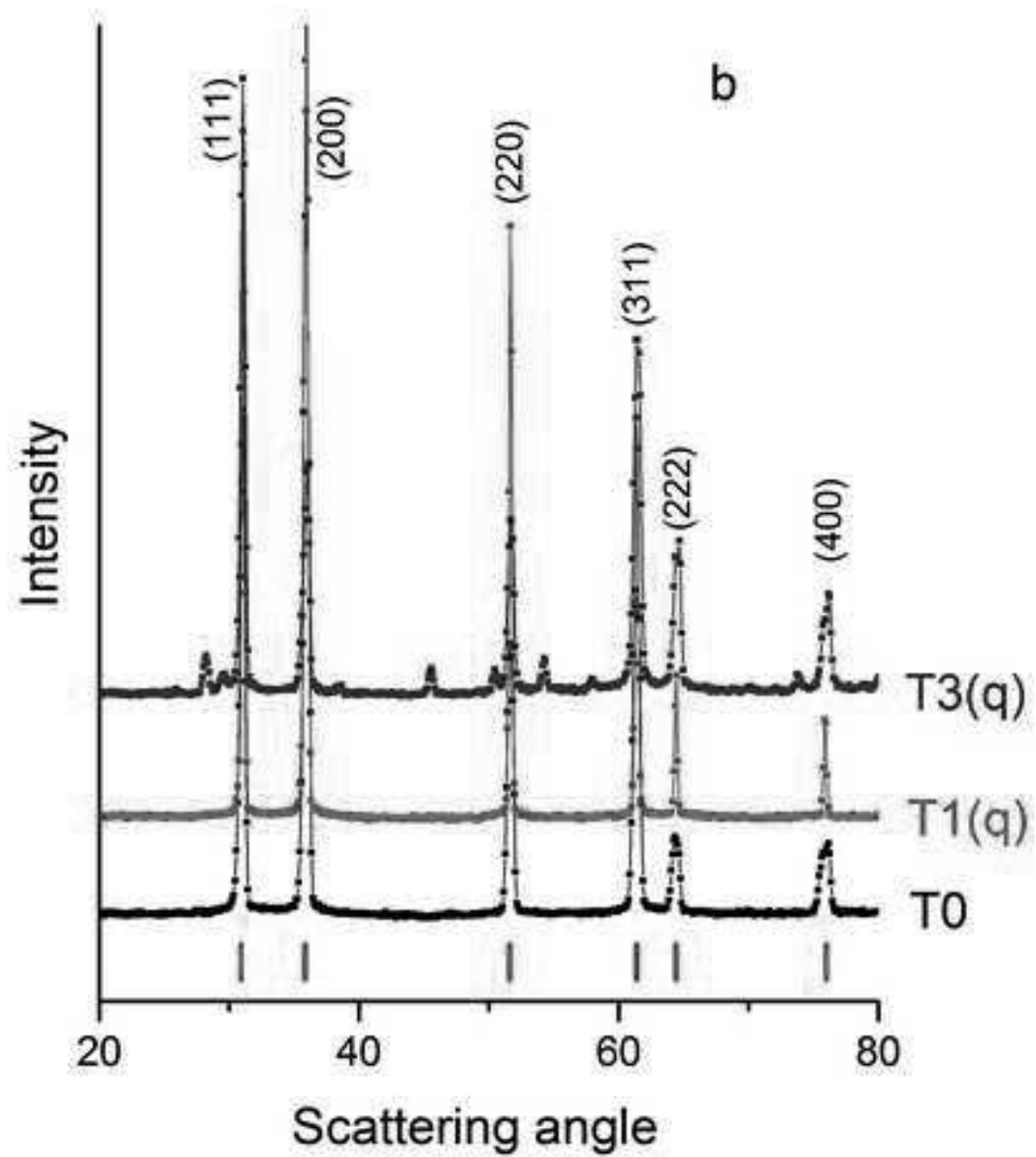


Figure  
Click here to download high resolution image

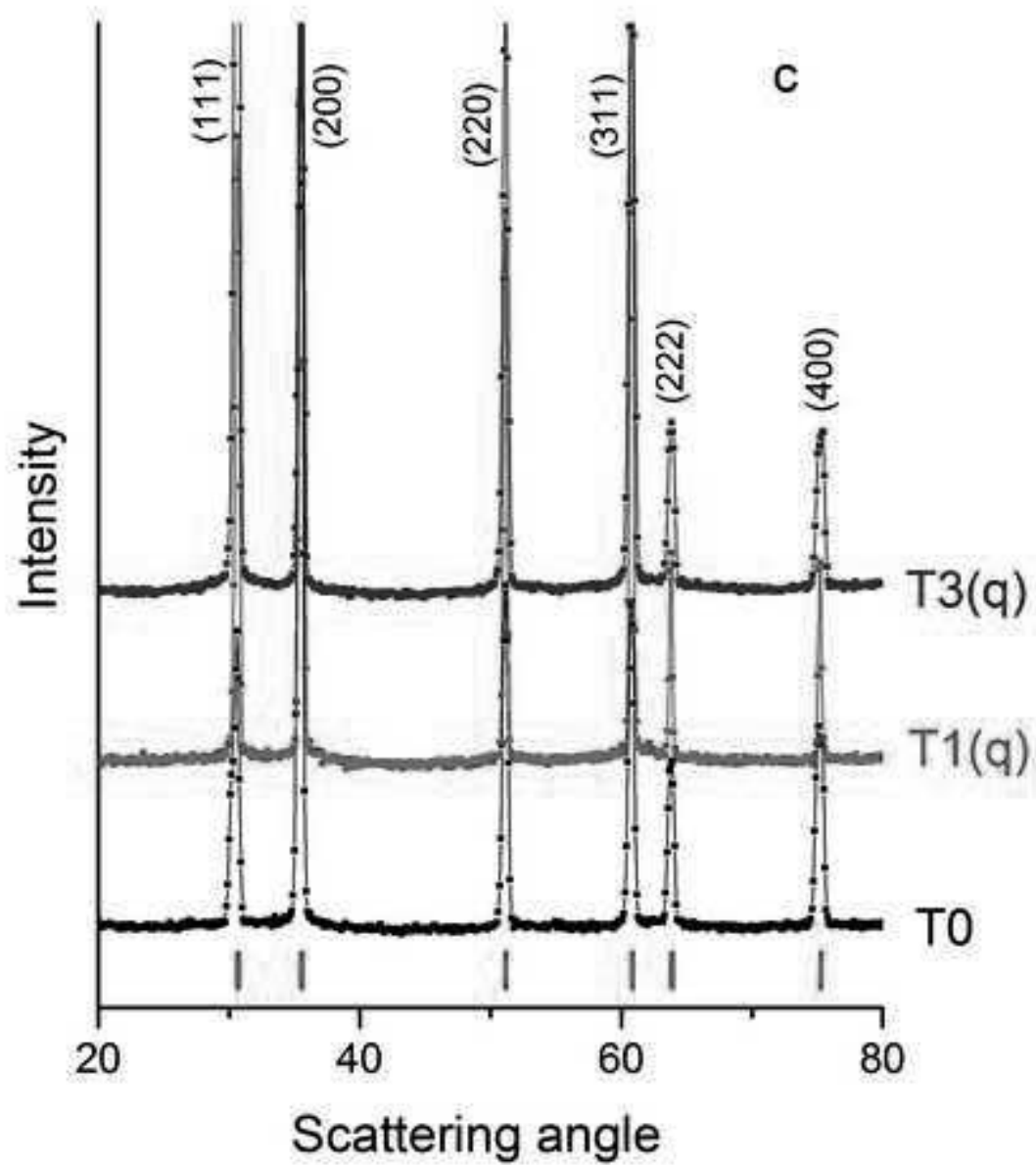


Figure  
[Click here to download high resolution image](#)

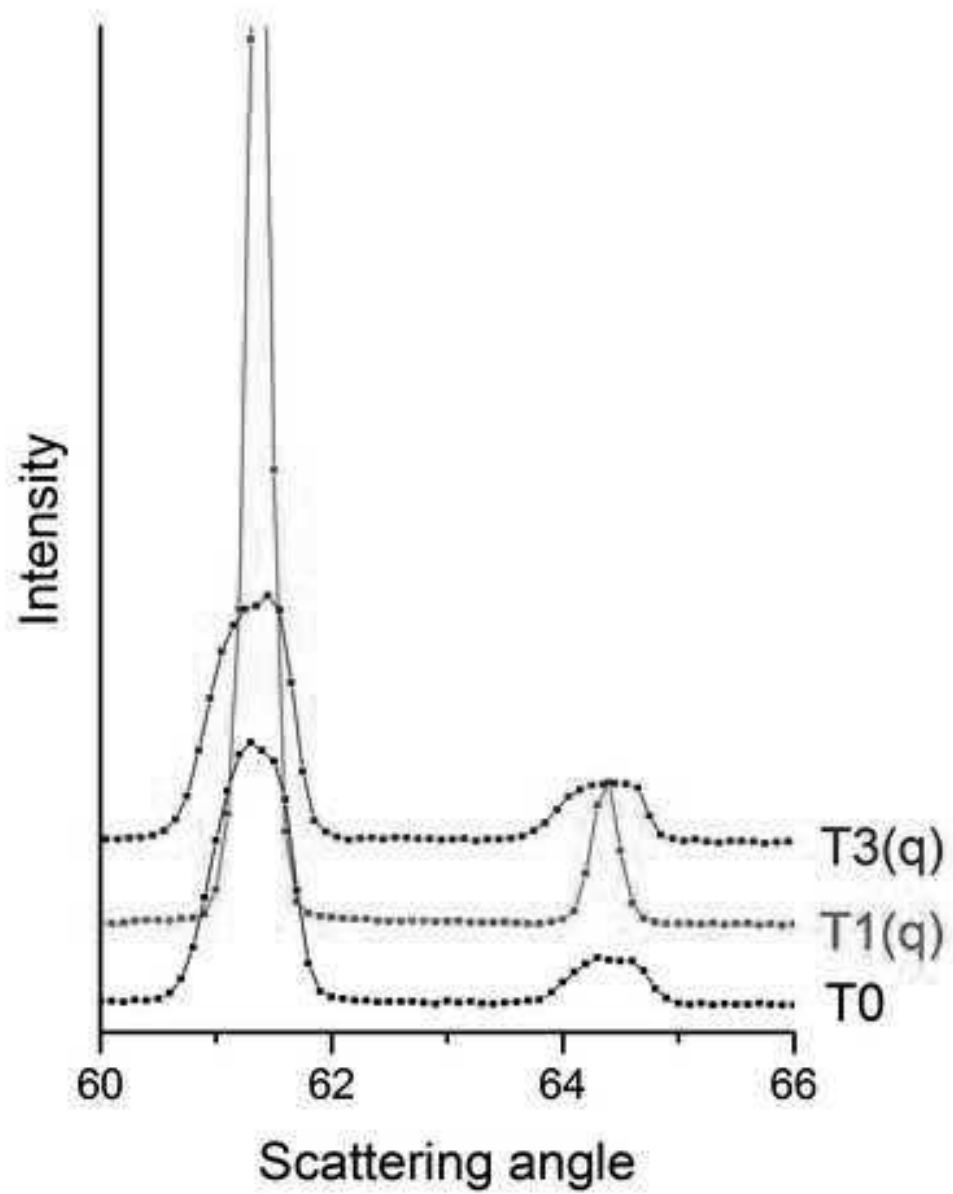


Figure  
Click here to download high resolution image

